Traditional Deformation Analysis and Octree-Based Deformation Analysis

Subjects: Others

Contributor: Lukas Fahle , Andrew J. Petruska , Gabriel Walton , Jurgen F. Brune , Elizabeth A. Holley

Convergence and rockmass failure are significant hazards to personnel and physical assets in underground tunnels, caverns, and mines. Mobile Laser Scanning Systems (MLS) can deliver large volumes of point cloud data at a high frequency and on a large scale.

mobile laser scanning | geotechnical monitoring | octree data structures | change detection | statistical inference

1. Introduction

During the excavation and operation of underground openings, such as caverns, tunnels, and mining drifts, the redistribution in their surrounding stress field tends to result in the closure, or so-called convergence, of these openings [1]. Geometric changes in the perimeter of the opening can also result in structural damage and rockmass instabilities. In underground cavern construction and operation, rockmass stability and deformation have been identified as key risks [2][3][4][5]. During tunnel excavations, wall deformation monitoring is critical for applications, including subsidence prevention, the New Austrian Tunneling Method (NATM), and observational excavation methods [6]. Deformations can also help predict more severe failures or be used for back analysis and support design refinements [7]. Convergence and rockmass failures, such as fall of ground, are also significant hazards to both personnel and physical assets in underground mines [8][9][10][11][12][13].

In cavern engineering, tunneling, mining, geotechnical monitoring, and ground control measures are implemented to detect and prevent convergence and fall of ground, thus ensuring safety, operational reliability, and economic viability. In large, complex, and dynamically changing underground openings, such as mines, ground fall and convergence hazards are commonly detected through visual inspections by trained mine personnel. In situ convergence monitoring instrumentation, such as extensometers, provides only local, not mine-wide data. Visual inspections or locally installed sensors do not offer mine-wide, accurate, and timely information about ground fall hazards. Additionally, in-person inspections, installation, and maintenance of spot sensors expose personnel to the same hazards they must monitor [14]. Similar limitations and risks apply to visual and spot monitoring in cavern and tunneling domains.

As an alternative, lidar-based Simultaneous Localization and Mapping (SLAM) Mobile Laser Scanning Systems (MLS) can enable frequent, large-scale geotechnical monitoring due to significantly higher data acquisition

efficiency than traditional inspections [15][16][17][18][19][20]. MLS can also offer safety benefits by removing operators from hazardous areas, as they can be integrated into autonomous robotic platforms such as quadruped robots or mining equipment [21]. Fahle et al. [22] showed that multi-epoch MLS data could detect geotechnical hazards while achieving data quality with uncertainty on the millimeter-to-centimeter level. MLS in underground mines has potential beyond geotechnical monitoring applications, including mapping and monitoring ground support performance [23], mine ventilation surveying [24], rock fragmentation analysis [25], and the control of autonomous vehicle applications [26].

Without ground surveyed control points, static and mobile laser scanning suffer from drift error, reducing site-level accuracy [22][27]. SLAM-specific techniques, including loop-closure and SLAM-based scan registration, significantly improve site-level accuracy. The main limitations of current MLS data for large-wide monitoring remain the low target-level precision in unprocessed point clouds compared to static lidar and the need for time-consuming manual processing and analysis. The target-level precision of MLS data is primarily limited by using compact, automotive-grade MLS lidar sensors. The poor usability of MLS data results from the high data volume, in combination with legacy workflows and algorithms. As a result, there is currently no unified and automated method of organizing, processing, and analyzing MLS data for geotechnical change monitoring, impeding practical adoptions in underground mines.

2. Traditional Deformation Analysis and Change Detection

Point cloud change detection and deformation analysis aim to classify and measure geometric differences between two co-registered scan epochs of the same scene [28]. Several studies have investigated deformation analysis methods in circular concrete-lined rail and highway tunnels. They primarily analyze static terrestrial laser scanning (TLS) data using mathematically parameterized geometric shapes like ellipses and rectellipses fitted to 2D cross-sections of point cloud data [7][29][30][31]. These global shape-fitting approaches do not perform optimally in mining environments for two main reasons: irregular drift shapes require relatively complex geometric models for parameterization, and irrelevant changes in the drift floor due to the addition or removal of material limit the amount of usable data [31]. These approaches are also not designed to identify discrete, localized failures such as roof fall and rib spalling [32]. While shape-fitting approaches have received attention in research, cloud-to-cloud (C2C) and cloud-to-mesh (C2M) have been some of the first to be employed for change detection in mining operations [33]. C2C provides fast computations but does not account for the directionality of change and is sensitive to point spacing and noise [34][35]. C2M distances, while providing directionally signed results, require computationally expensive meshing. C2M accuracy is also impacted by the quality of the mesh interpolation relative to the original surface [34]. Multi-scale model-to-model cloud comparison (M3C2) is a local averaging-based change detection method and does not require meshing as it operates directly on the point clouds. It calculates distances along a local normal vector estimated based on each point's neighborhood of a specified size. M3C2 then projects search cylinders along the normal vectors and calculates the locally averaged change between the two input clouds [36]. M3C2 is the current state-of-the-art in geomorphic point cloud-based change analysis, especially for low-frequency

TLS-based rock slope monitoring [37][38][39][40][41][42][43][44][45][46]. M3C2 and related methods have only seen limited use in the context of underground applications [31][47][48].

M3C2 change results can be used to identify statistically significant changes by estimating a “Level of Detection” [36], which is often underestimated on natural surfaces and, thereby, causes false negatives [35][44][49][50]. Winiwarter et al. [41] supplemented the M3C2 calculation with error propagation and covariance information. Their so-called M3C2-EP method demonstrates a lower level of detection than the original M3C2 implementation when tested on synthetic and field TLS data. Computational performance was not reported in the study. As M3C2-EP utilizes M3C2 with additional steps, its runtime is likely similar to, or higher than, M3C2. The M3C2-EP method requires additional metadata, such as sensor accuracy, alignment information, and scan positions. While M3C2 and its variants are more robust to noise than C2C and C2M, few studies have used it for mine-scale MLS-based change detection. Besides requiring extensive tuning for various data-sensor, application, and environment-dependent parameters, M3C2 and its variants’ main limitations for large-scale, complex, and mine-wide applications are their computational cost and resulting unsuitability for real-time processing.

3. Challenges in Large-Scale Mobile Laser Scanning Systems Data Analysis

MLS point cloud data for monitoring are high in volume, frequency, and variety and can be defined as big data. These properties present challenges for conventional data processing methodologies [51], such as the ones for change detection summarized in **Table 1**. Researchers' literature review presented studies that described their limitations regarding noise robustness and computational efficiency. In addition, researchers believe that their lack of topological structure and their natively non-classification-based change detection approach further limit their adoption for geotechnical monitoring.

Table 1. Properties of traditional change detection methods.

Method	Robust to Noise	Computationally Efficient	Topological Structure	Classification-Based	References
Shape Fitting	Yes	No	No	No	[7][29][30][31]
C2C	No	Yes	No	No	[34][35]
C2M	No	No	No	No	[34]
M3C2	Yes	No	No	No	[36]

C2C, C2M, and M3C2 results do not inherit 3D topological structures, such as information about spatially adjacent points. Instead, they output unstructured point cloud lists, similar to the input data format. The lack of topology makes the automation of 4D spatiotemporal analysis for underground convergence or rockfall challenging. Often time-consuming and error-prone visual interpretation is necessary to uncover regionally connected, time-dependent trends within the data. Additionally, the lack of topological structure makes traditional methods less

compatible with advanced applications for autonomous mobile platforms that require topological information to perceive and navigate their environment [26]. Shape-fitting methods can provide some basic abstraction, e.g., by outputting results as individual cross-sections [7]. Spatial clustering can be a post-processing method that provides additional topological context and has been used for rockfall detection [44][52].

Current point cloud deformation and change detection analysis commonly evaluate change based on a calculated distance between point clouds from different epochs. This distance is often displayed as a continuous variable for individual points using a color scale and legend. While this is sufficient for low-frequency visual analysis of small scenes, it creates challenges for high-frequency, mine-scale monitoring. Some of these are exemplified and illustrated in **Figure 1**. Due to sensor noise, most points show 0.05 m of change, which likely marks the limit of detection. While filtering these points is trivial, other scenarios are more challenging to solve for easier interpretation. For example, in **Figure 1**A, points with distances larger than 0.2 m have been colored in grey to help identify missing data between two scan epochs. In **Figure 1**B, the transition from missing data to available data results in points incorrectly showing up to 20 cm changes. In **Figure 1**C, where partial coverage between two scans exists, distinguishing real changes from missing data is challenging. Viewing angle ambiguity is another challenge in visual interpretation, especially for large-scale and dense data. In **Figure 1**D, changes in the drift floor are only visible when data are viewed at an oblique angle and might be false positives, as Walton et al. [31] discussed. A high number of potential false positives in the dataset can obscure true positives in the mine drift roof in **Figure 1**E.

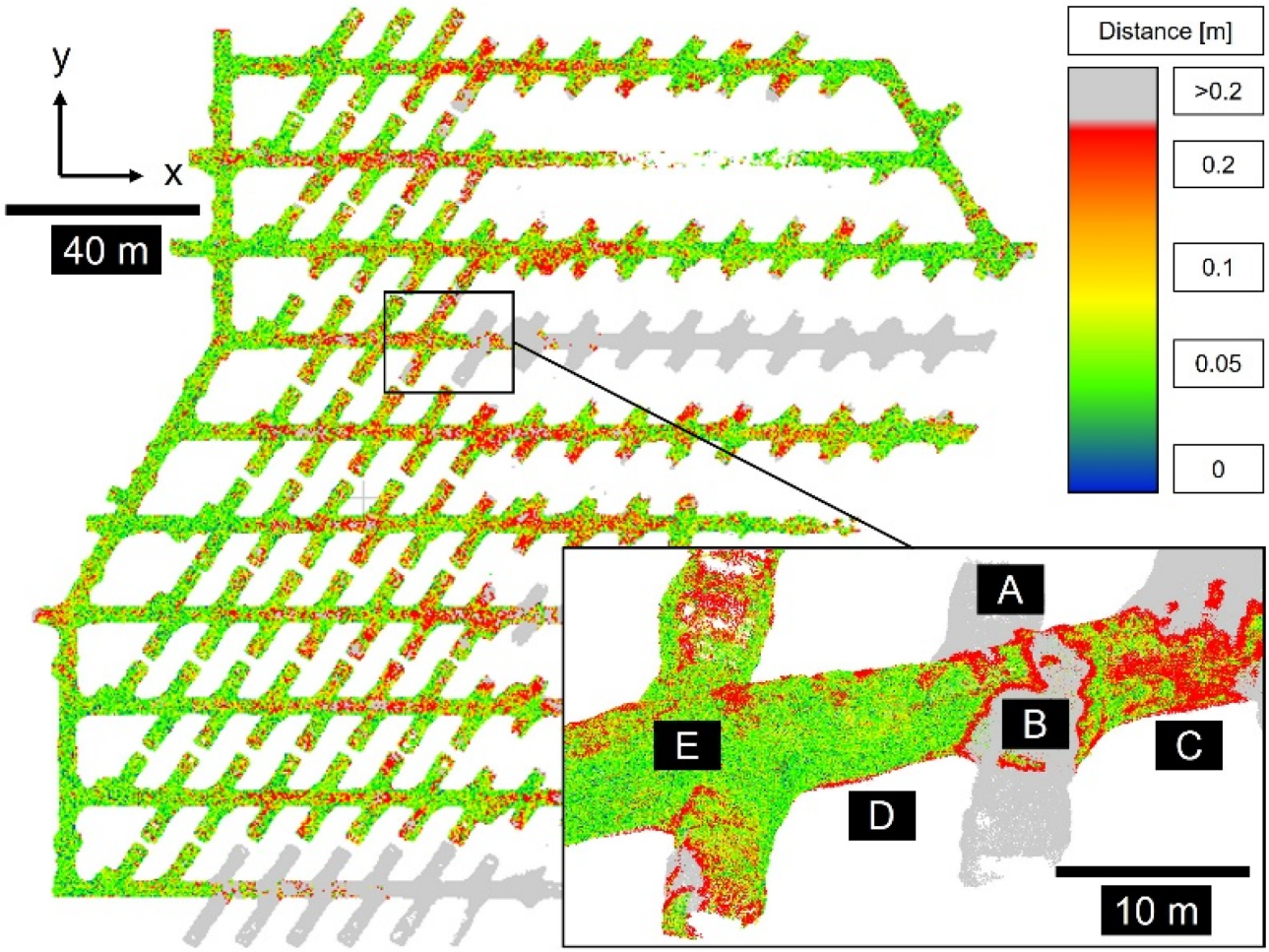

Figure 1. Example of color-coded lidar data of mine-wide changes by absolute distances. (**A**): Missing data, (**B**): Transition from missing data to available data, (**C**): Partial coverage between two scans, (**D**): Changes in drift floor, (**E**): Potential false positives in drift roof.

Visual interpretations are subjective, time-consuming, and error-prone and require manual steps to utilize results in business intelligence or automation workflows. For example, many mines utilize so-called Trigger Action Response Plans (TARPs) to manage geotechnical risks [53]. A TARP requires clearly defined alert levels based on real-time monitoring inputs or triggers, e.g., for a specific convergence rate. A classification-based change detection framework could incorporate mine-site-specific triggers and help eliminate delays and errors in the visual interpretation of monitoring data. A more automated, less subjective classification-based approach is desirable to improve the detection and differentiation of geotechnically relevant and significant changes.

Finally, a robust monitoring program must achieve a sufficient limit of detection. Critical convergence magnitudes with a potential negative impact on safety and productivity can be classified from 1–10%, i.e., 0.05 to 0.5 m of wall-to-wall convergence in a 5 m-wide drift [54]. Additionally, rockfall as small as 0.1 m in diameter has been shown to cause fatal injuries in underground mines [55]. For mine-wide monitoring of geotechnical hazards, researchers can assume that a practical limit of detection for convergence should at least be 0.05 m wall-to-wall change and 0.1 m edge-length for rockfall events.

4. Octree-Based Deformation Analysis and Change Detection

Several studies have undertaken underground deformation analysis using static lidar sensors. The previous section showed that MLS-based underground mine scale deformation and change detection provide opportunities to improve traditional approaches. As a core technology in robotic mapping [56], SLAM-based MLS [57], and point cloud data processing [34], voxel-based octree data structures could help solve the challenges traditional change detection methods face with mine-scale MLS data. An octree is a hierarchical data structure that divides 3D space into nodes [58][59]. Nodes are commonly represented by cubical volumes referred to as voxels. Each voxel can be recursively divided into eight smaller sub-sections until a minimum voxel size or tree depth is reached. The minimum voxel size l_{min} determines the octree's level of detail or resolution, with lower values representing higher resolutions. In robotic and laser-scanning applications, octree resolution is usually determined by available system memory, lidar sensor resolution, and application-specific requirements [56][60]. Additionally, lower resolutions of an octree can always be generated by performing cuts at any depth of the octree, making them multi-resolution. Lower octree resolution generally increases the speed of computational operations, such as tree-based searches [56]. In practice, l_{min} can, therefore, be selected as small as memory availability allows but is usually limited by lidar data resolution and processing speed requirements.

In applications that utilize point cloud data from laser scanners, a voxel is usually initialized by integrating a laser-scan measurement with an x, y, and z location. In this basic form, a voxel encodes a simple Boolean property to describe the occupancy state of its space. Octrees can encode additional information, such as three-dimensional ellipsoids or surfel representations. These can be particularly interesting when processing low-precision MLS data, as they can encode statistical descriptors such as the mean, variance, and covariance of the points in each voxel. These statistics describe sampled surfaces in more detail than a Boolean occupancy property (**Figure 2**). Voxel and surfels have been used to improve SLAM performance with examples in indoor [61][62] and larger urban environments [63][64]. Zlot and Bosse [65] demonstrated the efficiency of ellipsoid-supplemented voxels for large-scale underground mine mapping but did not investigate multi-temporal applications such as ground movement monitoring.

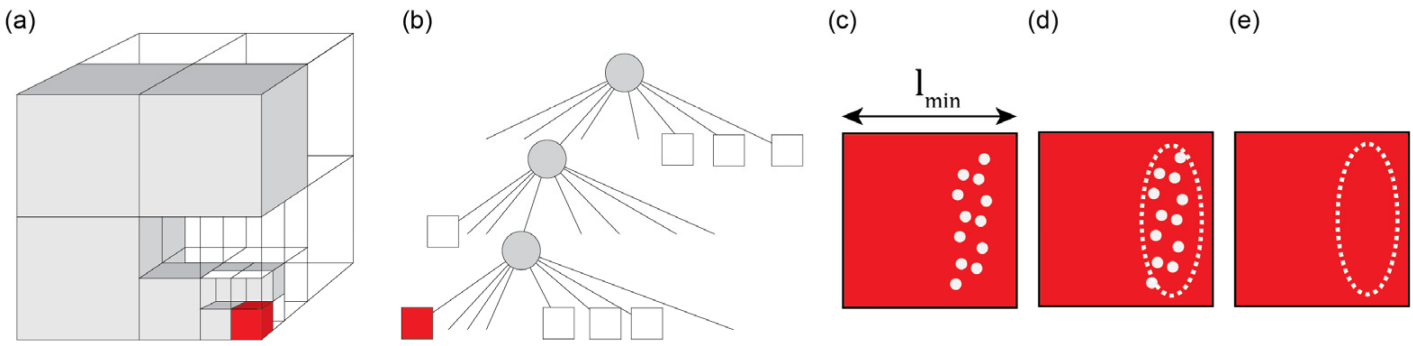

Figure 2. Schematic of a volumetric (**a**) and tree (**b**) representation of an octree structure storing Boolean occupancy free (white) and occupied (grey). Example of an occupied voxel of size l_{min} storing MLS points of a surface (**c**), a graphical representation of the covariance of the points (**d**), and the data maintained in researchers' octree (**e**).

Shortcomings of voxel-based representations include their susceptibility to discretization artifacts created when large, open scenes are not sufficiently observed and a loss in accuracy compared to the original point cloud data [66][67]. Underground mine environments present fewer discretization challenges due to their confined nature, high MLS sampling rates, and high point cloud density. The loss of accuracy remains a concern, especially in safety-critical monitoring applications. Gehrung et al. [68] address this in urban datasets by supplementing voxels with a local spatial data representation in the form of a three-dimensional Gaussian kernel. In a later version of their method, they detected the appearance and disappearance of objects like pedestrians and cars using a voxel edge length of 0.5 m [69]. Wellhausen et al. [70] presented a voxel-based change detection pipeline using distance computations, thresholding, clustering, and classification. Their approach detected objects larger than 0.5 m in real-time using a voxel edge length of 0.75 m. Gehrung et al.'s [69] and Wellhausen et al.'s [70] implementations of voxel-based change detection showed promising results in urban scenarios and for relatively high magnitudes of changes.

Previous voxel-based change detection work focused on relatively large and discrete changes in urban environments and often used high-accuracy lidar sensors. In contrast to these methods, researchers' proposed approach for underground geotechnical monitoring must handle noisy MLS data and provide a low detection limit, preferably below the MLS sensor-specific range accuracy. Researchers' approach must also accurately detect appearing objects characterized by high-magnitude changes in relatively small regions, such as the ones caused by rockfalls and low-magnitude, incremental deformation over larger regions associated with rockmass convergence. Unlike conventional change detection techniques employed in underground applications, researchers' method needs to produce a robust binary change classification with user-definable risk tolerance and absolute magnitudes of changes. Lastly, researchers aim to develop a framework that can be utilized for various underground mining applications that require a highly efficient and customizable data storage and processing platform.

References

1. Terzaghi, K. Shield tunnels of the Chicago Subway. J. Boston Soc. Civ. Eng. 1942, 29, 163–210.
2. Ma, K.; Zhang, J.; Zhou, Z.; Xu, N. Comprehensive analysis of the surrounding rock mass stability in the underground caverns of Jinping I hydropower station in Southwest China. Tunn. Undergr. Space Technol. 2020, 104, 103525.
3. Hu, Z.; Wu, B.; Xu, N.; Wang, K. Effects of discontinuities on stress redistribution and rock failure: A case of underground caverns. Tunn. Undergr. Space Technol. 2022, 127, 104583.
4. Li, S.; Yu, H.; Liu, Y.; Wu, F. Results from in-situ monitoring of displacement, bolt load, and disturbed zone of a powerhouse cavern during excavation process. Int. J. Rock Mech. Min. Sci. 2008, 45, 1519–1525.

5. Zhao, J.S.; Jiang, Q.; Lu, J.F.; Chen, B.R.; Pei, S.F.; Wang, Z.L. Rock fracturing observation based on microseismic monitoring and borehole imaging: In situ investigation in a large underground cavern under high geostress. Tunn. Undergr. Space Technol. 2022, 126, 104549.
6. Wittke, W.; Pierau, B.; Erichsen, C. New Austrian Tunneling Method (NATM)—Stability Analysis and Design; WBI: Essen, Germany, 2006.
7. Walton, G.; Delaloye, D.; Diederichs, M.S. Development of an elliptical fitting algorithm to improve change detection capabilities with applications for deformation monitoring in circular tunnels and shafts. Tunn. Undergr. Space Technol. 2014, 43, 336–349.
8. Kaiser, P.K.; Cai, M. Design of rock support system under rockburst condition. J. Rock Mech. Geotech. Eng. 2012, 4, 215–227.
9. Mark, C.; Molinda, G.M. Preventing falls of ground in coal mines with exceptionally low-strength roof: Two case studies. In Proceedings of the 23rd International Conference on Ground Control in Mining, Morgantown, WV, USA, 3–5 August 2004.
10. Nordlund, E. Deep hard rock mining and rock mechanics challenges. In Proceedings of the Ground Support 2013: The Seventh International Symposium on Ground Support in Mining and Underground Construction, Perth, Australia, 13 May 2013; pp. 39–56.
11. Oraee, K.; Oraee, N.; Goodarzi, A.; Khajehpour, P. Effect of discontinuities characteristics on coal mine stability and sustainability: A rock fall prediction approach. Int. J. Min. Sci. Technol. 2016, 26, 65–70.
12. Palei, S.K.; Das, S.K. Sensitivity analysis of support safety factor for predicting the effects of contributing parameters on roof falls in underground coal mines. Int. J. Coal Geol. 2008, 75, 241–247.
13. Sandbak, L.A.; Rai, A.R. Ground Support Strategies at the Turquoise Ridge Joint Venture, Nevada. Rock Mech. Rock Eng. 2013, 46, 437–454.
14. Centers for Disease Control and Prevention. NIOSH Mine and Mine Worker Charts. 2021. Available online: https://wwwn.cdc.gov/niosh-mining/MMWC (accessed on 2 September 2021).
15. Williams, K.; Olsen, M.J.; Roe, G.; Glennie, C. Synthesis of transportation applications of mobile LiDAR. Remote Sens. 2013, 5, 4652–4692.
16. Luo, X.; Ren, X.T.; Li, Y.; Wang, J.J. Mobile surveying system for road assets monitoring and management. In Proceedings of the 2012 7th IEEE Conference on Industrial Electronics and Applications (ICIEA), Singapore, 18–20 July 2012; pp. 1688–1693.
17. Puente, I.; Akinci, B.; González-Jorge, H.; Díaz-Vilariño, L.; Arias, P. A semi-automated method for extracting vertical clearance and cross sections in tunnels using mobile LiDAR data. Tunn. Undergr. Space Technol. 2016, 59, 48–54.

18. Raval, S.; Banerjee, B.P.; Singh, S.K.; Canbulat, I. A Preliminary Investigation of Mobile Mapping Technology for Underground Mining. In Proceedings of the IGARSS 2019–2019 IEEE International Geoscience and Remote Sensing Symposium, Yokohama, Japan, 28 July–2 August 2019; pp. 6071–6074.
19. Lynch, B.K.; Marr, J.; Marshall, J.A.; Greenspan, M. Mobile LiDAR-Based Convergence Detection in Underground Tunnel Environments. 2017. Available online: http://hdl.handle.net/1974/15638 (accessed on 17 May 2022).
20. Singh, S.K.; Banerjee, B.P.; Raval, S. A review of laser scanning for geological and geotechnical applications in underground mining. Int. J. Min. Sci. Technol. 2023, 33, 133–154.
21. Fahle, L.; Holley, E.; Walton, G. Toward a mine-wide, real-time, and autonomous geotechnical change detection, monitoring, and prediction framework for underground mines. In Proceedings of the 39th International Conference on Ground Control in Mining, ICGCM 2020, Canonsburg, PA, USA, 28–30 July 2020.
22. Fahle, L.; Holley, E.A.; Walton, G.; Petruska, A.J.; Brune, J.F. Analysis of SLAM-Based Lidar Data Quality Metrics for Geotechnical Underground Monitoring. Min. Metall. Explor. 2022, 39, 1939–1960.
23. Gallwey, J.; Eyre, M.; Coggan, J. A machine learning approach for the detection of supporting rock bolts from laser scan data in an underground mine. Tunn. Undergr. Space Technol. 2021, 107, 103656.
24. Watson, C.; Marshall, J. Estimating underground mine ventilation friction factors from low density 3D data acquired by a moving LiDAR. Int. J. Min. Sci. Technol. 2018, 28, 657–662.
25. Engin, I.C.; Maerz, N.H.; Boyko, K.J.; Reals, R. Practical Measurement of Size Distribution of Blasted Rocks Using LiDAR Scan Data. Rock Mech. Rock Eng. 2020, 53, 4653–4671.
26. Marshall, J.; Barfoot, T.; Larsson, J. Autonomous underground tramming for center-articulated vehicles. J. Field Robot. 2008, 25, 400–421.
27. Jones, E.; Ghabraie, B.; Beck, D. A method for determining field accuracy of mobile scanning devices for geomechanics applications. In Proceedings of the ISRM International Symposium—10th Asian Rock Mechanics Symposium, ARMS 2018, Singapore, 29 October–3 November 2018; pp. 978–981.
28. Lindenbergh, R.; Pietrzyk, P. Change detection and deformation analysis using static and mobile laser scanning. Appl. Geomat. 2015, 7, 65–74.
29. Wannenmacher, H.; Krenn, H.; Komma, N.; Tunnel, A.S. Improved pressure tunnel lining methods, a case study of the Niagara Tunnel Facility Project. In World Tunnel Congress 2013, Geneva; Anagnostou, G., Ehrbar, H., Eds.; CRC Press: London, UK, 2013.

30. Nuttens, T.; Stal, C.; de Backer, H.; Schotte, K.; van Bogaert, P.; de Wulf, A. Methodology for the ovalization monitoring of newly built circular train tunnels based on laser scanning: Liefkenshoek Rail Link (Belgium). Autom. Constr. 2014, 43, 1–9.
31. Walton, G.; Diederichs, M.S.; Weinhardt, K.; Delaloye, D.; Lato, M.J.; Punkkinen, A. Change detection in drill and blast tunnels from point cloud data. Int. J. Rock Mech. Min. Sci. 2018, 105, 172–181.
32. Han, J.Y.; Guo, J.; Jiang, Y.S. Monitoring tunnel deformations by means of multi-epoch dispersed 3D LiDAR point clouds: An improved approach. Tunn. Undergr. Space Technol. 2013, 38, 385–389.
33. Fekete, S.; Diederichs, M.; Lato, M. Geotechnical and operational applications for 3-dimensional laser scanning in drill and blast tunnels. Tunn. Undergr. Space Technol. 2010, 25, 614–628.
34. Girardeau-Montaut, D.; Roux, M.; Marc, R.; Thibault, G. Change Detection on Points Cloud Data Acquired with A Ground Laser Scanner. In Proceedings of the ISPRS WG III/3, III/4, V/3 Workshop “Laser Scanning 2005”, Enschede, The Netherlands, 12–14 September 2005.
35. Barnhart, T.B.; Crosby, B.T. Comparing two methods of surface change detection on an evolving thermokarst using high-temporal-frequency terrestrial laser scanning, Selawik River, Alaska. Remote Sens. 2013, 5, 2813–2837.
36. Lague, D.; Brodu, N.; Leroux, J. Accurate 3D comparison of complex topography with terrestrial laser scanner: Application to the Rangitikei canyon (N-Z). ISPRS J. Photogramm. Remote Sens. 2013, 82, 10–26.
37. Williams, J.G.; Rosser, N.J.; Hardy, R.J.; Brain, M.J.; Afana, A.A. Optimising 4-D surface change detection: An approach for capturing rockfall magnitude-frequency. Earth Surf. Dyn. 2018, 6, 101–119.
38. van Veen, M.; Hutchinson, D.J.; Kromer, R.; Lato, M.; Edwards, T. Effects of sampling interval on the frequency—magnitude relationship of rockfalls detected from terrestrial laser scanning using semi-automated methods. Landslides 2017, 14, 1579–1592.
39. Kromer, R.A.; Abellán, A.; Hutchinson, D.J.; Lato, M.; Edwards, T.; Jaboyedoff, M. A 4D filtering and calibration technique for small-scale point cloud change detection with a terrestrial laser scanner. Remote Sens. 2015, 7, 13029–13058.
40. Bonneau, D.A.; Hutchinson, D.J. The use of terrestrial laser scanning for the characterization of a cliff-talus system in the Thompson River Valley, British Columbia, Canada. Geomorphology 2019, 327, 598–609.
41. Winiwarter, L.; Anders, K.; Höfle, B. M3C2-EP: Pushing the limits of 3D topographic point cloud change detection by error propagation. ISPRS J. Photogramm. Remote Sens. 2021, 178, 240–258.

42. Abellán, A.; Jaboyedoff, M.; Oppikofer, T.; Vilaplana, J.M. Detection of millimetric deformation using a terrestrial laser scanner: Experiment and application to a rockfall event. Nat. Hazards Earth Syst. Sci. 2009, 9, 365–372.
43. Abellán, A.; Oppikofer, T.; Jaboyedoff, M.; Rosser, N.J.; Lim, M.; Lato, M.J. Terrestrial laser scanning of rock slope instabilities. Earth Surf. Process. Landf. 2014, 39, 80–97.
44. DiFrancesco, P.M.; Bonneau, D.; Hutchinson, D.J. The implications of M3C2 projection diameter on 3D semi-automated rockfall extraction from sequential terrestrial laser scanning point clouds. Remote Sens. 2020, 12, 1885.
45. Kromer, R.A.; Hutchinson, D.J.; Lato, M.J.; Gauthier, D.; Edwards, T. Identifying rock slope failure precursors using LiDAR for transportation corridor hazard management. Eng. Geol. 2015, 195, 93–103.
46. Lato, M.J.; Diederichs, M.S.; Hutchinson, D.J.; Harrap, R. Evaluating roadside rockmasses for rockfall hazards using LiDAR data: Optimizing data collection and processing protocols. Nat. Hazards 2012, 60, 831–864.
47. Evans, P. Improving Convergence Monitoring Using Lidar Data At Rio Tinto'S Argyle Diamond Mine Improving Convergence Monitoring Using Lidar Data at Rio Tinto'S Argyle Diamond Mine. 2021, pp. 1–12. Available online: https://www.emesent.io/2021/05/26/improving-convergence-monitoring-using-lidar-data-at-rio-tintos-argyle-diamond-mine/ (accessed on 21 March 2023).
48. Vanneschi, C.; Mastrorocco, G.; Salvini, R. Assessment of a rock pillar failure by using change detection analysis and FEM modelling. ISPRS Int. J. Geo-Inf. 2021, 10, 774.
49. Benjamin, J.; Rosser, N.; Brain, M. Rockfall detection and volumetric characterisation using LiDAR. In Landslides and Engineered Slopes. Experience, Theory and Practice; CRC Press: Boca Raton, FL, USA, 2016; Volume 2, pp. 389–395.
50. Ozdogan, M.V.; Deliormanli, A.H. Landslide detection and characterization using terrestrial 3D laser scanning (LIDAR). Acta Geodyn. Geomater. 2019, 16, 379–392.
51. Gandomi, A.; Haider, M. Beyond the hype: Big data concepts, methods, and analytics. Int. J. Inf. Manag. 2015, 35, 137–144.
52. Tonini, M.; Abellan, A. Rockfall detection from terrestrial lidar point clouds: A clustering approach using R. J. Spat. Inf. Sci. 2014, 8, 95–110.
53. Sharon, R.; Eberhardt, E. Guidelines for Slope Performance Monitoring; CSIRO Publishing: Collingwood, Australia, 2020.
54. Mercier-Langevin, F.; Hadjigeorgiou, J. Towards a better understanding of squeezing potential in hard rock mines. Min. Technol. 2011, 120, 36–44.

55. Mark, C.; Iannacchione, A.T. Best Practices to mitigate injuries and fatalities from rock falls. In Proceedings of the 31st Annual Institute on Mining Health, Safety and Research, Roanoke, Virginia, 27–30 August 2000; pp. 115–129. Available online: https://stacks.cdc.gov/view/cdc/8586 (accessed on 14 August 2022).
56. Hornung, A.; Wurm, K.M.; Bennewitz, M.; Stachniss, C.; Burgard, W. OctoMap: An efficient probabilistic 3D mapping framework based on octrees. Auton. Robot. 2013, 34, 189–206.
57. Zhang, J.; Singh, S. Low-drift and real-time lidar odometry and mapping. Auton. Robot. 2017, 41, 401–416.
58. Wilhelms, J.; van Gelder, A. Octrees for faster isosurface generation. ACM Trans. Graph. 1992, 11, 201–227.
59. Meagher, D. Geometric modeling using octree encoding. Comput. Graph. Image Process. 1982, 19, 129–147.
60. Berrio, J.S.; Zhou, W.; Ward, J.; Worrall, S.; Nebot, E. Octree map based on sparse point cloud and heuristic probability distribution for labeled images. In Proceedings of the 2018 IEEE/RSJ International Conference on Intelligent Robots and Systems (IROS), Madrid, Spain, 1–5 October 2018.
61. Park, C.; Moghadam, P.; Kim, S.; Elfes, A.; Fookes, C.; Sridharan, S. Elastic LiDAR Fusion: Dense Map-Centric Continuous-Time SLAM. In Proceedings of the IEEE International Conference on Robotics and Automation, Brisbane, Australia, 21–25 May 2018.
62. Whelan, T.; Leutenegger, S.; Salas-Moreno, R.F.; Glocker, B.; Davison, A.J. ElasticFusion: Dense SLAM without a pose graph. Robot. Sci. Syst. 2015, 11, 1–9.
63. Behley, J.; Stachniss, C. Efficient Surfel-Based SLAM using 3D Laser Range Data in Urban Environments. Robot. Sci. Syst. XIV 2018, 2018, 59.
64. Droeschel, D.; Behnke, S. Efficient continuous-time SLAM for 3D lidar-based online mapping. In Proceedings of the 2018 IEEE International Conference on Robotics and Automation (ICRA), Brisbane, Australia, 21–25 May 2018; pp. 5000–5007.
65. Zlot, R.; Bosse, M. Efficient Large-Scale 3D Mobile Mapping and Surface Reconstruction of an Underground Mine; Springer Tracts in Advanced Robotics: Heidelberg, Germany, 2014; Volume 92, pp. 479–494.
66. Gehrung, J.; Hebel, M.; Arens, M.; Stilla, U. A Voxel-Based Metadata Structure for Change Detection in Point Clouds of Large-Scale Urban Areas. ISPRS Ann. Photogramm. Remote Sens. Spat. Inf. Sci. 2018, 4, 97–104.
67. Xu, Y.; Tong, X.; Stilla, U. Voxel-based representation of 3D point clouds: Methods, applications, and its potential use in the construction industry. In Automation in Construction; Elsevier B.V.:

Amsterdam, The Netherlands, 2021; Volume 126.

68. Gehrung, J.; Hebel, M.; Arens, M.; Stilla, U. A fast voxel-based indicator for change detection using low resolution octrees. ISPRS Ann. Photogramm. Remote Sens. Spat. Inf. Sci. 2019, 4, 357–364.
69. Gehrung, J.; Hebel, M.; Arens, M.; Stilla, U. Change Detection and Deformation Analysis Based on Mobile Laser Scanning Data of Urban Areas. ISPRS Ann. Photogramm. Remote Sens. Spat. Inf. Sci. 2020, 5, 703–710.
70. Wellhausen, L.; Dube, R.; Gawel, A.; Siegwart, R.; Cadena, C. Reliable real-time change detection and mapping for 3D LiDARs. In Proceedings of the SSRR 2017—15th IEEE International Symposium on Safety, Security and Rescue Robotics, Shanghai, China, 11–13 October 2017; pp. 81–87.